Advances in Physics: X

ISSN: (Print) 2374-6149 (Online) Journal homepage: http://www.tandfonline.com/loi/tapx20

Josephson plasmonics in layered superconductors

Y. Laplace & A. Cavalleri

To cite this article: Y. Laplace & A. Cavalleri (2016): Josephson plasmonics in layered superconductors, Advances in Physics: X, DOI: 10.1080/23746149.2016.1212671

To link to this article: http://dx.doi.org/10.1080/23746149.2016.1212671

Published online: 02 Aug 2016.

ADVANCES IN PHYSICS: X, 2016
http://dx.doi.org/10.1080/23746149.2016.1212671

Taylor & Francis
Taylor & Francis Group

REVIEW ARTICLE

OPEN ACCESS

Josephson plasmonics in layered superconductors

Y. Laplace[a] and A. Cavalleri[a,b]

[a]Max Planck Institute for the Structure and Dynamics of Matter, Hamburg, Germany; [b]Department of Physics, Clarendon Laboratory, Oxford University, Oxford, UK

ABSTRACT

We review the optical physics of Josephson plasmons in cuprate superconductors. These coherent charge modes arise from tunneling of the superfluid between superconducting planes and exhibit strong nonlinearities and quantum coherent dynamics at THz frequencies. We summarize early transport and microwave experiments in $Bi_2Sr_2CaCu_2O_{8+\delta}$ (BSCCO) and discuss more recent work performed in $La_{2-x}Sr_xCuO_4$ (LSCO) and $La_{2-x}Ba_xCuO_4$ (LBCO) using nonlinear THz techniques. We cover THz-driven oscillations between superconducting and resistive states, optical excitation of solitonic breathers, and the parametric amplification of Josephson plasma waves. The last part of the review discusses some new research directions, including cooling of superconducting phase fluctuations with lasers and optical cavity control techniques.

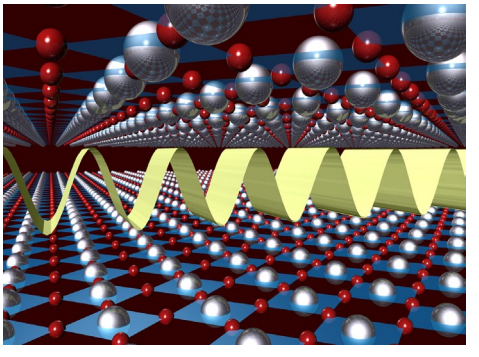

ARTICLE HISTORY
Received 11 March 2016
Accepted 23 June 2016

KEYWORDS
Superconductivity; plasmonics; terahertz

PACS
74.72.-h cuprate superconductors; 74.25.Gz optical properties; 74.50.+r tunneling phenomena, Josephson effects; 74.40. Gh Nonequilibrium superconductivity

1. Introduction

The superconducting transition involves the formation of electron pairs, which condense below a critical transition temperature (T_c) and determine DC and

CONTACT A. Cavalleri andrea.cavalleri@mpsd.mpg.de

low-frequency AC transport. A single condensate wavefunction is reflected in a complex order parameter $\Delta(x, y, z, t)e^{i\chi(x,y,z,t)}$, with an amplitude $\Delta(x, y, z, t)$ and a phase $\chi(x, y, z, t)$. Due to the breaking of gauge symmetry that leads to superconductivity, this order parameter exhibits a rigid phase, which resists deformation in space and time.

At equilibrium and without external perturbation, energy is minimized if the order parameter amplitude and phase are constant in space and time ($\Delta(x, y, z, t) = \Delta$ and $\chi(x, y, z, t) = 0$). Perturbative excitations of the order parameter around this equilibrium can be described as distortions of the amplitude Δ (sometimes referred to as the Higgs amplitude mode of the order parameter) and of the phase (Goldstone modes of the superconductor).

Phase modes can be understood as longitudinal plasma excitations of the $2e$ Cooper pairs, which are coupled through the long range Coulomb interaction. As a consequence of Coulomb interaction, these modes acquire a finite excitation frequency for long wavelengths. The frequency of the plasma modes is related to the superfluid density ρ_s as $\omega_p^2 \propto \rho_s$. In general, both uncondensed normal carriers and the superconducting fluid participate to the plasma response in conventional superconductors, and signatures of the low-density superconducting plasma are difficult to detect. However, in layered superconductors, like high-T_c cuprates [1], normal-state transport is incoherent (insulating) along the c-axis, so that no metallic plasmon is visible in that direction. Hence, when superconducting tunneling sets in for $T < T_c$, distinctive features appear, reflecting the superconducting plasma alone.

An interlayer superconducting plasma mode is for example observed at GHz–THz frequencies for most cuprates (see Figure 1). The frequency is low because the superfluid density is reduced by the tunneling. As a consequence, the out-of-plane rigidity of the phase is small and susceptible to phase fluctuations of the order parameter [2,3].

Pioneering experiments have detected signatures of Josephson tunneling in current–voltage (I–V) measurements along the c-axis of $Bi_2Sr_2CaCu_2O_{8+\delta}$ (BSCCO)

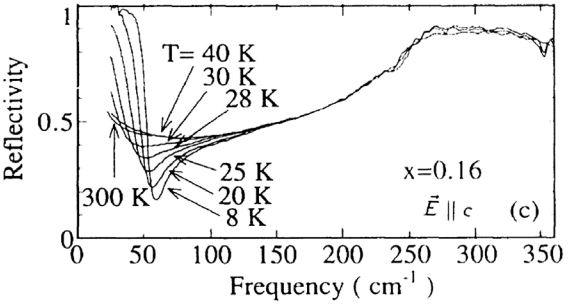

Figure 1. Infrared reflectivity spectra of the optimally doped $La_{2-x}Sr_xCuO_4$ for $x = 0.16$ ($T_c = 34$ K) with polarization perpendicular to the CuO_2 planes (E//c) for different temperatures above and below T_c. Reprinted with permission from Tamasaku et al. [4]. Copyright 1992 by the American Physical Society.

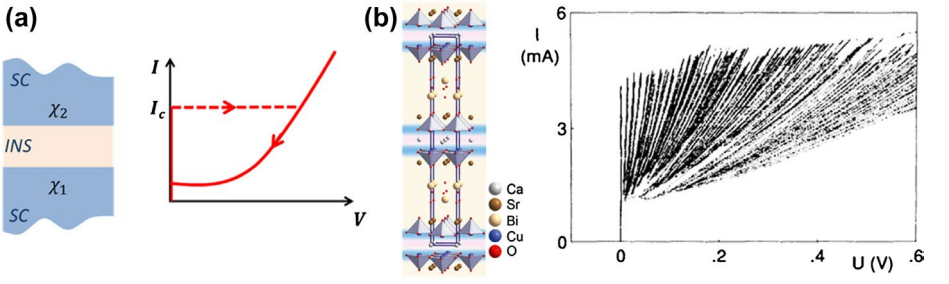

Figure 2. (a) A conventional Josephson junction, where $\chi_{1,2}$ are the phases of the superconducting order parameter in each superconductor (SC = superconductor; INS = insulating barrier). Sketch of the *I–V* characteristic of an under-damped Josephson junction. (b) Unit cell of the high-T_c cuprate $Bi_2Sr_2CaCu_2O_{8+\delta}$ (BSCCO) with the CuO_2 planes shown as blue layers. Experimental *I–V* characteristic of a bulk BSCCO sample below T_c. Reprinted with permission from Kleiner et al. [5]. Copyright 1992 by the American Physical Society.

and other high-T_c cuprates [5,6]. Especially important in these early experiments is the observation of multiple branches in the *I–V* curves, characteristic of the response of a stack of Josephson junctions connected in series (see Figure 2). Other aspects of the Josephson effect have also become observable, including microwave emission via the AC–Josephson effect, Shapiro steps, the Fraunhofer-type dependence of the Josephson critical current in magnetic fields, and macroscopic quantum tunneling of the Josephson phase [7,8]. Hence, high-T_c cuprates should be considered as two-dimensional layered materials with superconducting CuO_2 planes which are weakly coupled via Josephson tunneling through insulating barriers. The superconducting order parameter is appropriately described if we consider a constant order parameter amplitude throughout the material $\Delta(x,y,z,t) = \Delta$ and a set of phases $\{\varphi_n(x,y,t)\}_{n=1,\ldots,N}$, in which each phase $\varphi_n(x,y,t)$ describes the phase difference of the Josephson junction made of two neighboring superconducting layers [9].

Let us recall the physics of a single Josephson junction, made up of two bulk superconductors separated by a thin insulator (see Figure 2(a)). The gauge invariant phase difference is defined as $\varphi = \chi_2 - \chi_1 + \frac{2e}{\hbar}\int_1^2 \vec{A}.\vec{dl}$, with χ_1 and χ_2 denoting the phases of the order parameters in each superconductor and $\vec{A}$ the vector potential. The two Josephson relations are: $\partial_t\varphi = \frac{2e}{\hbar}V(t)$ and $I = I_c\sin(\varphi)$, with $V(t)$ representing the voltage drop between the two superconductors and I_c the critical current of the junction.

In long Josephson junctions, where the spatial dependence of the phase in the directions perpendicular to the junction has to be taken into account, the two Josephson relations are supplemented with Maxwell's equations, and, in one-dimension, $\varphi(x,t)$ follows a sine-Gordon equation [10]:

$$\frac{1}{\omega_p^2}\frac{\partial^2\varphi}{\partial t^2} - \lambda_J^2\frac{\partial^2\varphi}{\partial x^2} + \sin(\varphi) = 0 \qquad (1)$$

Here, λ_J is the Josephson penetration depth, ω_p is the Josephson plasma resonance (JPR) frequency, and $c_0 = \lambda_J \omega_p$ is the Swihart velocity.

For a stack of intrinsic Josephson junctions (IJJ) composed of N superconducting layers, a similar derivation can be performed and the dynamics of the phases $\{\varphi_n(x,t)\}_{n=1,\ldots,N-1}$ is described by a set of coupled sine-Gordon equations with appropriate boundary conditions [11–14]. The coupling between different junctions is inductive and arises from the screening of the in-plane magnetic field by the superconducting currents. The in-plane magnetic screening length in cuprates (e.g. $\lambda_{ab} \sim 100$ nm in BSCCO) is notably larger than the thickness of a single CuO_2 plane (Å scale); hence, in a single junction, the magnetic flux is never screened, with field lines extending over a large number of unit cells.

A special case occurs when the Josephson phase does not depend on space within the *ab*-plane and $\varphi_n(x,t) = \varphi_n(t)$. This happens for instance when no magnetic field is present within the stack and/or if the dimensions of the stack in the *ab*-plane are smaller than the magnetic penetration depth. In this case, the superconducting phase excitations are longitudinal, i.e. the electric field lies along the direction of propagation of the wave. Coupling between the junctions arises in this context due to charging of the superconducting layers, i.e. is capacitive.

1.1. Zero frequency: Meissner effect and the Josephson vortex lattice

If one ignores time dependence, Equation (1) reads:

$$-\lambda_J^2 \frac{\partial^2 \varphi}{\partial x^2} + \sin(\varphi) = 0 \tag{2}$$

When a magnetic field is applied to the junction, this equation describes the screening of the magnetic field by the superconducting Josephson currents, as detailed below.

In the short junction limit ($L \ll \lambda_J$, L being the lateral dimension of the junction), where a magnetic flux can thread the junction, the Fraunhofer-type dependence of the Josephson critical current is observed, both for a single Josephson junction and for a stack of IJJ [6,15].

For long junctions ($L \gtrsim \lambda_J$) and small applied fields ($<<H_{c1}$), where $\sin(\varphi) \sim \varphi$, the solution takes the form $\varphi \sim e^{-x/\lambda_J}$. In this case, the applied magnetic field is expelled from the inside of the junction and directed toward its edges, i.e. it is effectively screened by the Josephson currents.

For large fields ($>H_{c1}$), Equation (2) describes the magnetic flux penetration in the form of Josephson vortices, in which the Josephson currents are positive and negative as the phase sweeps $[0, 2\pi]$ intervals, driving a tunneling current in a vortex loop. In the case of the stack of IJJ, Josephson vortices spread over more than one junction, and inductive coupling arranges the Josephson vortices in a lattice. Figure 3 shows a Josephson vortex in a conventional Josephson junction and a

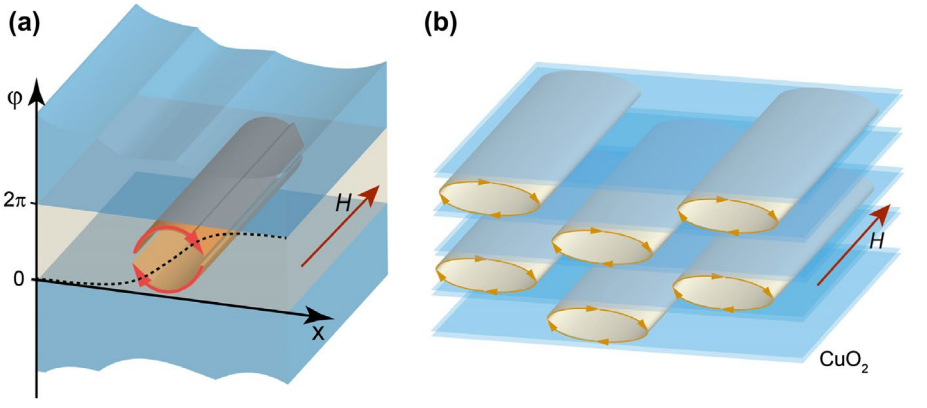

Figure 3. (a) Sketch of a Josephson vortex in a long Josephson junction induced by a magnetic field H. The spatial dependence of the Josephson phase $\varphi(x)$ is shown as a dashed line. Red arrows indicate the superconducting current flow. (b) Sketch of a triangular Josephson vortex lattice in high-T_c superconductors.

Josephson vortex lattice in the case of a stack of IJJ. Contrary to the case of in-plane Abrikosov vortices (for magnetic fields applied along the c-axis), Josephson vortices do not possess a 'normal core', as they are centered in the insulating barrier (for further review on vortices in high-T_c superconductors, see [16] and [17]).

1.2. Finite frequency: emission of THz radiation

One of the most interesting consequences of the physics discussed above is the emission of THz radiation for the application of a DC current (for further review, see [18], [19] and references therein). Radiation of electromagnetic waves is rooted in the AC Josephson effect described by the nonlinear *RLC* circuit model of the Josephson junction (Figure 4) [10].

By taking Equation (1) in the short junction limit (i.e. removing the spatial dependence), under the application of a DC bias current I and by adding a damping term β, we obtain:

$$\frac{1}{\omega_p^2}\frac{\partial^2\varphi}{\partial t^2} + \beta\frac{\partial\varphi}{\partial t} + \sin(\varphi) = \frac{I}{I_c} \tag{3}$$

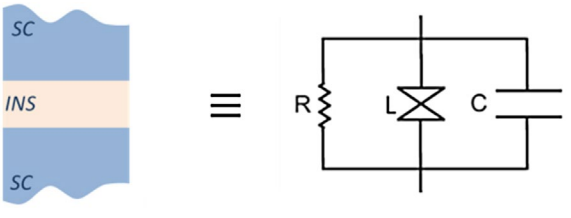

Figure 4. Equivalent circuit model of a short Josephson junction.

In this model, the junction is described by a nonlinear inductance L (which describes the Josephson coupling between the superconducting layers), a capacitance C (the capacitive coupling between the superconducting layers), and a resistance R (due to the finite conductivity of the non-condensed quasi-particles), with $\omega_p = 1/\sqrt{LC}$ and $\beta = L/R$.

Below the critical current $I < I_c$, this equation has a solution $\varphi(t) = \varphi_0$ which is time independent. Physically, the junction is in the zero resistance state, where superconducting carriers 'short' the normal carriers.

When the junction has been biased above its critical current I_c, oscillations of the tunneling current appear. The junction develops a finite voltage V_{dc} for which, according to the first Josephson relation, the phase evolves as $\varphi(t) = \frac{2e}{\hbar} V_{dc} t$. Consequently, the Josephson current $I(t) = I_c \sin\left(\frac{2e}{\hbar} V_{dc} t\right)$ oscillates at a frequency $\nu = \frac{2e}{h} V_{dc}$ and radiation is emitted.

However, for emission of intense THz radiation in stacks of IJJ, all phases must be synchronized, a requirement that is not always easily fulfilled [20–27].

To describe synchronization and strong THz emission [28] (see Figure 5), we take the continuum limit of the coupled sine-Gordon equations and we replace the discrete index of the junction n by the continuous variable z (corresponding to the direction of the c-axis) so that $\{\varphi_n(x,t)\}_{n=1,\ldots,N} \to \varphi(x,z,t)$. In the linear regime ($\sin(\varphi) \sim \varphi$), this yields [29]:

$$\left(1 - \lambda_{ab}^2 \frac{\partial^2}{\partial z^2}\right)\left(\frac{1}{\omega_p^2}\frac{\partial^2 \varphi}{\partial t^2} + \varphi\right) - \lambda_c^2 \frac{\partial^2 \varphi}{\partial x^2} = 0 \tag{4}$$

where λ_{ab} and λ_c are the magnetic penetration depths for screening currents running within the CuO_2 layers and along the c-axis, respectively. Accordingly, propagating solutions of the type $\varphi \sim e^{i(k_x x + k_z z - \omega t)}$, i.e. Josephson plasma waves (JPW), satisfy the following dispersion relation: $\omega^2 = \omega_p^2\left(1 + \frac{\lambda_c^2 k_x^2}{1 + \lambda_{ab}^2 k_z^2}\right)$.

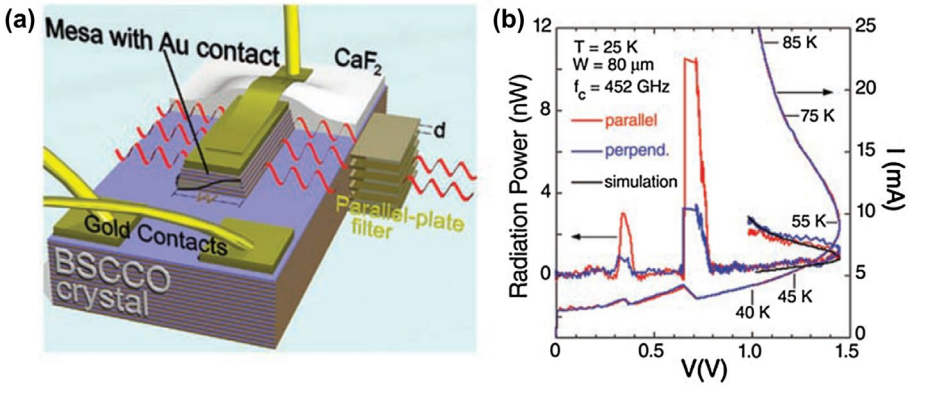

Figure 5. BSCCO mesa used for THz emission via the AC Josephson effect (left) and *I*–*V* characteristic of the BSCCO mesa superimposed with the corresponding radiated power (right). From Ozyuzer et al. [28]. Reprinted with permission from AAAS.

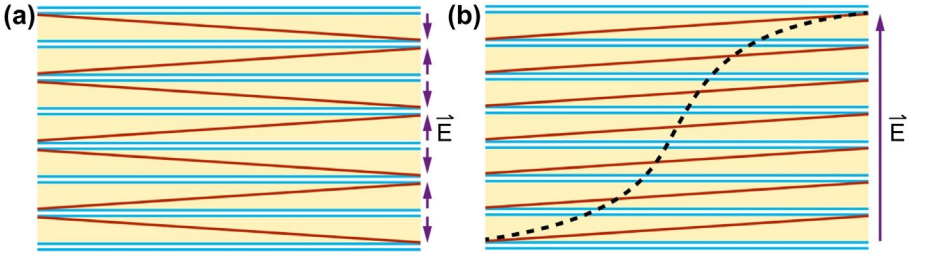

Figure 6. Two different JPW modes in a stack of IJJ. (a) out-of-phase JPW with alternating phases of the waves from junction to junction. (b) in-phase JPW. Arrows indicate electric fields at the edge of the stack. Electric fields corresponding to the out-of-phase JPW mode cancel each other, whereas they add up to produce intense THz radiation in the case of the in-phase JPW mode (adapted from Ozyuzer et al. [28]).

One finds that JPW have a frequency that depends not only on their propagation vector k_x along the junctions, but also on the out-of-plane propagation vector k_z. Figure 6 represents two of such modes for a stack of IJJ with lateral size L: the in-phase JPW ($k_x = \pi/L, k_z = 0$) and the out-of phase JPW ($k_x = \pi/L, k_z = \frac{\pi}{d}$, with d being the interlayer distance).

Because of their different resonant frequencies, the voltage drop V_{dc} across the junctions can be chosen so as to excite the in-phase JPW mode only with the resonance condition $\nu_{in-phase} = \frac{2e}{h}V_{dc}$. This mode, in turn, is the one that emits efficiently THz radiation because the phases of the whole stack of IJJ are synchronized.

1.3. Optical excitation of Josephson plasma modes

To describe the optical properties of the IJJ, we use the same continuum description given previously. We consider optical fields at $k \approx 0$, which cannot excite a short wavelength JPW mode (Figure 6(a)). For radiation at normal incidence, we have $k_z = 0$ so that the different Josephson phases of the stack are excited in-phase ($\varphi_n(x,t) = \varphi(x,t)$ for every n) and their dynamics behave as in the case of a single Josephson junction in the limit of $\lambda_J \to \lambda_c$ [30]:

$$\frac{1}{\omega_p^2}\frac{\partial^2\varphi}{\partial t^2} - \lambda_c^2\frac{\partial^2\varphi}{\partial x^2} + \varphi = 0 \tag{5}$$

The first two terms of Equation (5) describe wave propagation at velocity $\omega_p * \lambda_c = c/\sqrt{\epsilon_\infty}$, that is, at the speed of light in the material (ϵ_∞ is the dielectric constant of the insulating barrier at THz frequencies). Also, for plane waves of the type $\varphi \sim e^{i(k_x x - \omega t)}$, the dispersion relation takes the form : $k_x^2 = \frac{\epsilon_\infty}{c^2}\left(\omega^2 - \omega_p^2\right)$ For $\omega < \omega_p$, the wave vector k_x becomes imaginary and wave propagation inside

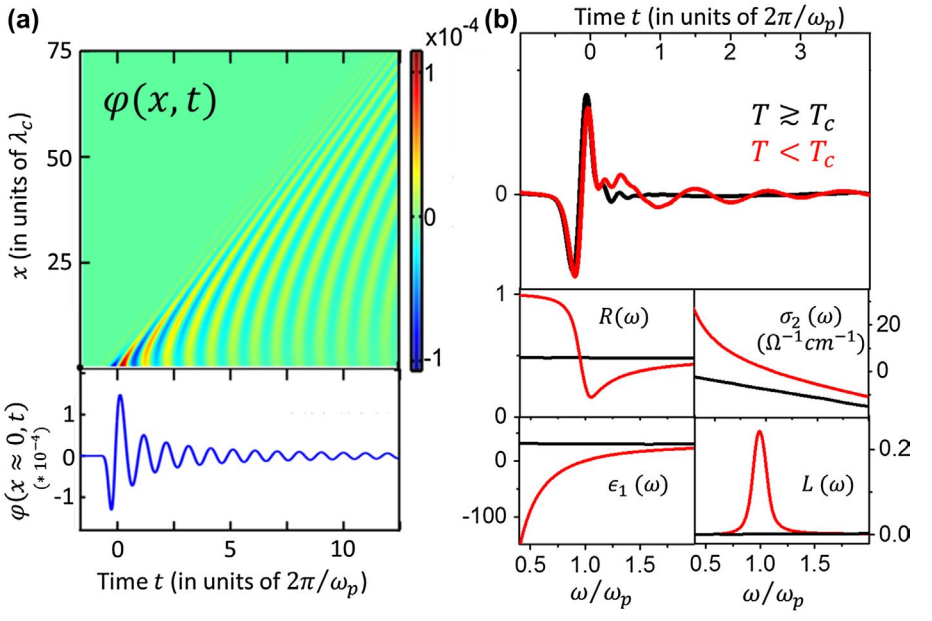

Figure 7. *Left:* simulation of the Equation (5) with appropriate boundary conditions for the time-dependent electromagnetic field at the surface of the superconductor Dienst et al. [30]. The color plot shows the Josephson phase as a function of time t and depth x inside the superconductor ($x = 0$ represents the surface boundary). The bottom panel is the corresponding time evolution of the Josephson phase for a line cut close to the surface boundary. *Right: c*-axis optical properties associated with the JPR phenomenon as probed with THz time domain spectroscopy above T_c (black solid curves) and below T_c (red curves).

the material is forbidden due to screening. For $\omega > \omega_p$, JPW can propagate inside the material.

We display below (Figure 7) the calculated space- and time-dependent phase oscillations excited by a single-cycle THz pulse [31]. The evolution of the Josephson phase $\varphi(x, t)$ is shown on a color scale as a function of time t and depth x inside the material. The THz pulse after reflection, displaying oscillations at frequency ω_p that are absent for $T > T_c$, is shown in the right panel of Figure 7.

The optical properties can be extracted from the THz time trace. Below T_c, the appearance of a narrow peak (delta function) in the real part of the conductivity $\sigma_1(\omega)$ implies that $\sigma_2(\omega)$ diverges as $\sim \omega_p^2/\omega \propto \rho_s/\omega$ (ρ_s is the superfluid density). The dielectric permittivity $\varepsilon_1(\omega)$ evolves from positive to negative values when the temperature T crosses T_c.

Finally, the loss function $L(\omega) = -\mathrm{Im}(1/\varepsilon(\omega))$, which peaks where $\varepsilon_1(\omega)$ crosses zero, displays a Lorentzian resonance centered at $\omega = \omega_p$, with a width that reflects damping and inhomogeneities in the Josephson coupling that can be either static or dynamic [32].

Additional Josephson plasma excitations exist in multilayer cuprates (e.g. in BSCCO, $YBa_2Cu_3O_{7-\delta}$ (YBCO), or Hg-based cuprates) as they possess more than

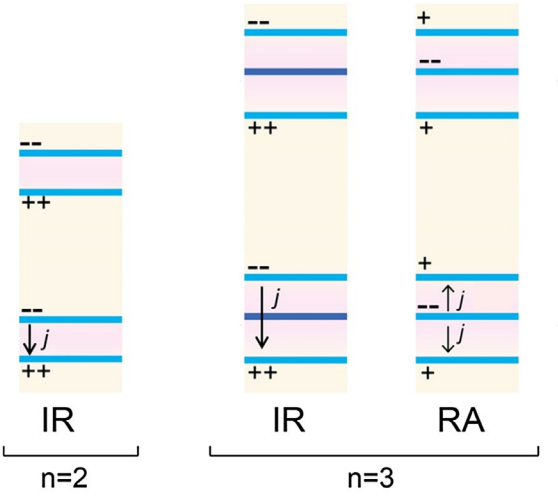

Figure 8. Classification of infrared active (IR) and Raman active (RA) longitudinal Josephson plasma modes in the intralayer region for bilayer ($n = 2$) and trilayer ($n = 3$) cuprates, where the superconducting layers are shown in blue. The corresponding Josephson currents (j) and charge distributions (++/− −) are indicated (adapted from Munzar and Cardona [36]).

one superconducting layer per unit cell. The dynamics of the intralayer excitations can be probed at mid-infrared frequencies and the optical nature of the different modes can be classified as either Raman or infrared active [33–37]. Examples of such intralayer excitations are shown in Figure 8 in the case of bilayer and trilayer cuprates.

Interestingly, the high-frequency intrabilayer Josephson plasma mode of YBCO, although highly damped, seems to appear for temperatures $T > T_c$, suggesting the existence of preformed Cooper pairs in the intrabilayer region [38]. This may in particular explain recent experiments which have shown the possibility to redistribute spectral weight between the interbilayer and intrabilayer modes by driving of a c-axis phonon mode, effectively resulting in a restoration of the superconducting coupling in the low-frequency Josephson junction above T_c. [39–41]

1.4. Surface Josephson plasma waves, linear and nonlinear THz optics

We conclude this introduction by mentioning some theoretical works addressing other types of linear and nonlinear Josephson plasma excitations. As discussed above, linear JPW propagating within the stack of IJJ are forbidden for frequencies below the JPR ($\omega < \omega_p$). However, surface plasma waves that propagate with frequencies below the plasma frequency exist. These cannot be excited with light impinging from free space directly and can only be driven through special methods, such as the use of a prism with total internal reflection [42], a periodic spatial modulation [43,44], the tip of an atomic force microscope (AFM) [45], and spatially confined geometries [46] (see Figure 9).

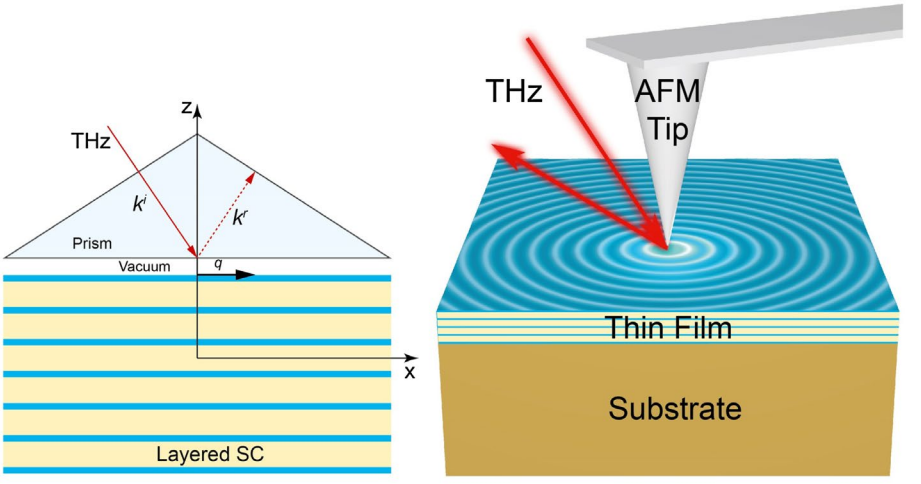

Figure 9. Two proposals for the coupling of incident THz radiation to launch and detect surface Josephson plasma waves in thin films of high-T_c cuprates: prism coupling (left, adapted from Slipchenko et al. [42]) and AFM tip coupling (right, adapted from Stinson et al. [45]).

A particularly interesting prospect lies in the possibility of using high-T_c cuprates as a tunable nonlinear medium to realize various types of analogs of nonlinear optics at THz frequencies [29] (consider for instance Equation (4) to be in the nonlinear regime). This includes, among others, the use of the Josephson vortex lattice as a photonic crystal for THz waves [47,48], negative index metamaterials [49], self-induced transparency, and optical bistability at THz frequencies [50–52].

2. Ultrafast and non-dissipative control of Josephson plasma phenomena with THz light pulses

As discussed above, Josephson plasma phenomena in cuprate superconductors can be controlled statically using a DC electric bias current [5,6] and/or magnetic fields [53,54]. This type of excitation inherently involves dissipation and heating effects are unavoidable. In the following, we discuss how the Josephson phase can be manipulated with strong THz frequency pulses. This allows for an ultrafast, yet, non-dissipative, mean of controlling Josephson plasma phenomena. In these experiments, the THz pump and probe pulses are polarized along the c-axis to drive and monitor the dynamics of the Josephson phase. Depending on the characteristics of the light excitation, different phenomena are observed.

2.1. Superconducting-resistive oscillations at THz frequencies

In the case where the frequency spectrum of the incident THz pump pulse E_{pump} (t) is below the JPR frequency, the pump pulse is screened within the penetration depth, where it drives the Josephson phase $\varphi(t)$ to high amplitudes according

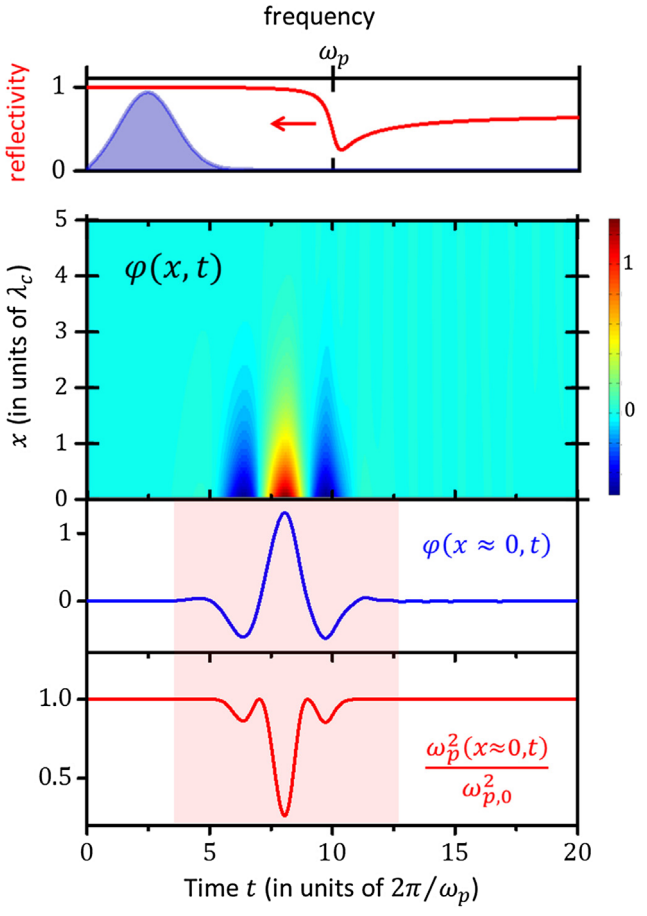

Figure 10. Simulations of the spatiotemporal dynamics of the Josephson phase $\varphi(x,t)$ after interaction with a broadband THz pulse with a frequency content located below the JPR. Top panel: Comparison between the Fourier spectrum of the THz pulse (purple area) and the JPR characterized by a plasma edge in the reflectivity (red curve). Main panel: two-dimensional color plot of the spatiotemporal evolution of $\varphi(x,t)$. Bottom panels: Time evolution of $\varphi(x \approx 0,t)$ and of the Josephson coupling $\omega_p^2(x \approx 0,t)/\omega_{p,0}^2$ for a line cut close to the surface boundary ($x \approx 0$). The red area marks the time during which the THz pump pulse is interacting with the superconductor.

to $\partial_t \varphi(t) = 2eV(t)/\hbar \propto E_{\text{pump}}(t)$ (see Figure 10). This allows for the control of the interlayer Josephson coupling, which depends on the Josephson phase as $\omega_p^2(t) = \omega_{p,0}^2 \cos(\varphi(t))$ ($\omega_{p,0}$ is the equilibrium JPR frequency). Importantly, under this non-resonant excitation, the superconducting coupling is modulated only within the duration of the pump pulse, returning to its initial state after the pump pulse has excited the sample.

Experimentally, this was achieved with an intense single-cycle THz pulse of central frequency ~450 GHz [55] used to drive the single layer cuprate $La_{1.84}Sr_{0.16}CuO_4$ $\left(T_c = 36\text{K}, \omega_p \sim 2\text{ THz}\right)$. [56] The time-dependent optical conductivity $\sigma_{ab/c}(\omega, t)$ within the penetration depth was determined with a delayed THz probe pulse. Although the in-plane optical conductivity $\sigma_{ab}(\omega, t)$ remained unchanged,

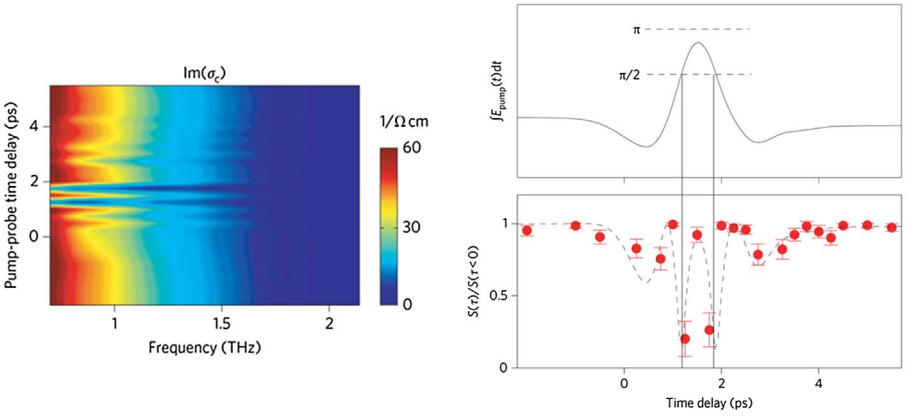

Figure 11. *Left*: Frequency-resolved optical conductivity $Im[\sigma_c(\omega,t)]$ as a function of pump–probe delay t at $T = 5$ K. *Right*: *top* Time evolution of the integral of the electric field of the THz pump pulse. *Bottom* Time evolution of the strength of the interlayer superconducting coupling quantified by $S(t)/S(t<0)$ where $S(t) = \lim_{\omega\to 0}\omega Im[\sigma_c(\omega,t)] = \omega_p^2(t)$ (red dots). The dashed line is a fit to the data points by a function of the form $\left|\cos(\alpha\int^t E_{\text{pump}}(\tau)d\tau)\right|$ where α is an adjustable parameter. Reprinted from Dienst et al. [56].

demonstrating the preservation of the in-plane superconducting properties, the THz pulse was found to periodically modulate the out-of-plane conductivity (see Figure 11, left panel). The imaginary part of the c-axis conductivity $Im[\sigma_c(\omega, t)]$ was found to oscillate in time, periodically vanishing (t = 1.25 ps, 1.75 ps) and recovering (t = 1.5 ps, $t > 2$ ps). Correspondingly, the real part of the conductivity $Re[\sigma_c(\omega, t)]$ increased (t = 1.25 ps, 1.75 ps) and vanished (t = 1.5 ps, $t > 2$ ps) periodically (not shown here). The strength of the superconducting coupling was experimentally determined by the time evolution of the inductive response $S(t)/S(t<0) = \lim_{\omega\to 0}\omega Im[\sigma_c(\omega,t)]/\omega_{p,0}^2 = \omega_p^2(t)/\omega_{p,0}^2$under the action of the THz electric field (Figure 11, right panel).

As expected from the previous discussion, this can be fitted with a function of the form $\left|\cos(\alpha\int^t E_{\text{pump}}(\tau)d\tau)\right|$, where α is a constant left as a free parameter in the analysis. For a strong enough THz field, as the phase $\varphi(t)$ advances in time, the superconducting coupling $\omega_p^2(t)$ acquires successively its maximum values for $\varphi(t) \approx 0$ (equilibrium) and for $\varphi(t) \approx \pi$ while it becomes vanishingly small when crossing $\varphi(t) \approx \frac{\pi}{2}$. At this phase value, where disruptive interference makes the supercurrent go to zero, transport occurs only through the uncondensed quasi-particles and the interlayer coupling is switched from superconducting to metallic. Additionally, the frequency of these superconducting-resistive oscillations was found to scale with the strength of the THz pulse above a certain threshold, a situation which is effectively reminiscent of the AC Josephson effect [56].

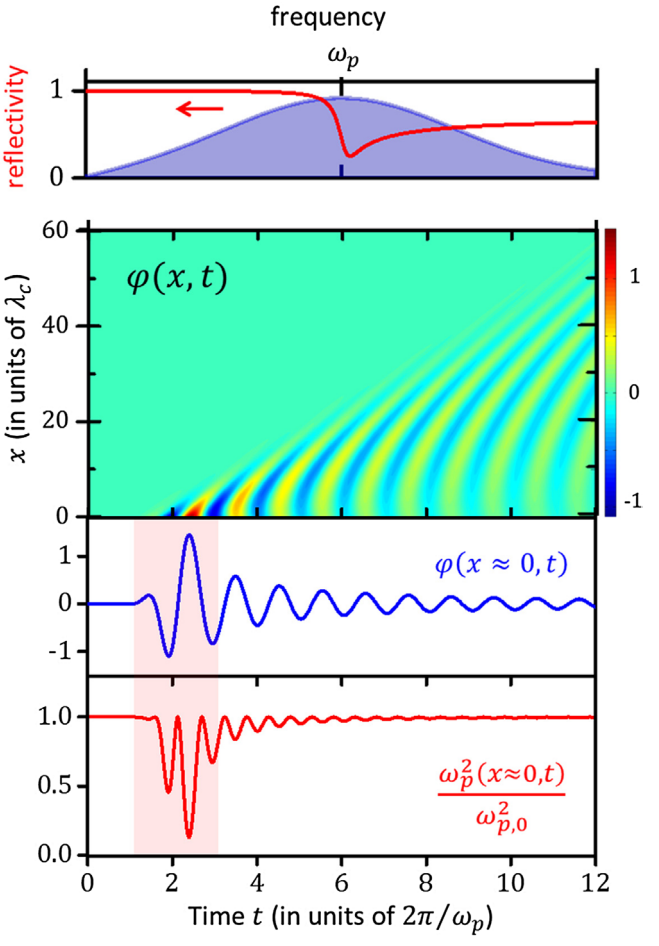

Figure 12. Simulations of the spatiotemporal dynamics of the Josephson phase $\varphi(x,t)$ after interaction with a broadband THz pulse with a frequency content resonant with the JPR. *Top panel*: Comparison between the Fourier spectrum of the THz pulse (purple area) and the JPR characterized by a plasma edge in the reflectivity (red curve). *Main panel*: two-dimensional color plot of the spatiotemporal evolution of $\varphi(x,t)$. *Bottom panels*: Time evolution of $\varphi(x \approx 0,t)$ and of the Josephson coupling $\omega_p^2(x \approx 0,t)/\omega_{p,0}^2$ for a line cut close to the surface boundary ($x \approx 0$). The red area marks the time during which the THz pump pulse is interacting with the superconductor.

2.2. *Parametric amplification of Josephson plasma waves*

When the THz pump pulse is tuned resonantly with the JPR, high-amplitude Josephson plasma waves are excited and propagate within the depth of the superconductor (see Figure 12). When expressing the oscillation of the Josephson phase as $\varphi(t) = \varphi_0 \cos\left(\omega_{p,0} t\right)$, one finds that $\omega_p^2(t) = \omega_{p,0}^2 \cos(\varphi(t)) \approx \omega_{p,0}^2\left[1 - \frac{\varphi_0^2}{4} - \frac{\varphi_0^2}{4}\cos\left(2\omega_{p,0} t\right)\right]$. Two main effects are expected: an average reduction of the interlayer coupling strength and a modulation at *twice* the frequency of the JPR.

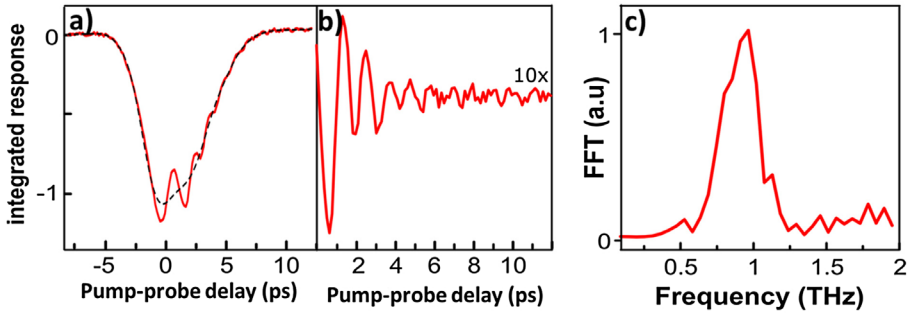

Figure 13. (a) pump–probe response for the frequency-integrated THz probe pulse as a function of pump–probe delay. (b) The fast oscillatory part of the signal is obtained by subtraction of the slow component shown as the black dashed line in panel a. (c) Fourier transform of the fast oscillatory signal shown in (b). Adapted from Rajasekaran et al. [57].

This was observed experimentally in the single layer cuprate $La_{1.905}Ba_{0.095}CuO_4$ (T_c = 32 K), chosen for its JPR frequency of ~500 GHz to be resonant with the THz pump pulse [57]. When plotting the spectrally integrated THz response, which is proportional to the total oscillator strength of the plasma resonance, these measurements display an average reduction of the oscillator strength and an oscillatory modulation (see Figure 13).

Importantly, the oscillatory response (Figure 13(b)) occurs at a frequency of ~1 THz (Figure 13(c)), i.e. *twice* the JPR frequency (~500 GHz), as expected.

The most interesting implication of this type of modulation of the JPR appears in the time- and frequency-dependent loss function as measured by the THz probe pulse. The loss function becomes successively negative and positive as a function of pump–probe delay, which corresponds, respectively, to amplification and deamplification of the Josephson plasma waves excited by the THz probe

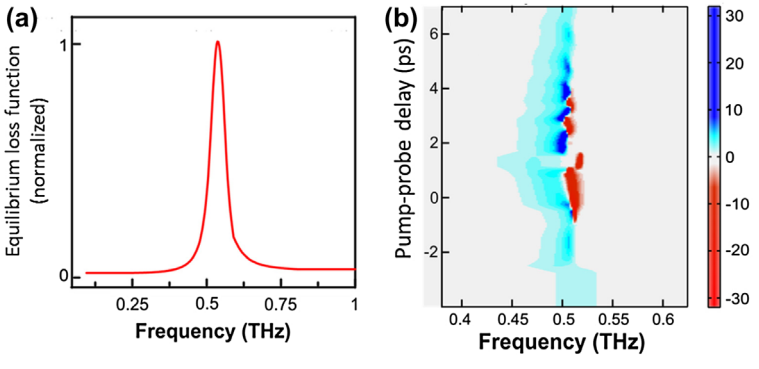

Figure 14. *Left panel*: normalized equilibrium loss function in the superconducting state of $La_{1.905}Ba_{0.095}CuO_4$ (T_c = 32 K). *Right panel*: Two-dimensional plot representing the time evolution of the frequency-resolved loss function as a function of pump–probe delay. Adapted from Rajasekaran et al. [57].

pulse (Figure 14). These alternating amplification/deamplication processes occur at twice the JPR frequency, consistent with the previous observations.

This phenomenon is easily understood if we take the Josephson phase to be a sum of the phases driven by the THz pump and THz probe pulses. When $\varphi(t) = \varphi_{\text{pump}}(t) + \varphi_{\text{probe}}(t)$, with $\varphi_{\text{pump}}(t) = \varphi_0 \cos(\omega_{\text{p,0}}t)$, the effective equation of motion describing the dynamics of $\varphi_{\text{probe}}(t)$ reads [30]:

$$\frac{\partial^2 \varphi_{\text{probe}}(t)}{\partial t^2} + \omega_{p,0}^2 \left[1 - \frac{\varphi_0^2}{4} - \frac{\varphi_0^2}{4}\cos\left(2\omega_{p,0}t\right)\right]\varphi_{\text{probe}}(t) = 0 \tag{6}$$

This equation of motion describes the dynamics of the oscillator $\varphi_{\text{probe}}(t)$ whose natural frequency is parametrically modulated at twice this frequency ($2\omega_{p,0}$), and resembles the Mathieu equation for a parametric amplifier. Consequently, amplification/deamplification occurs depending on the relative phase between the modulation and the Josephson oscillations, i.e. as a function of pump–probe delay in the experiments. These observations were also quantitatively reproduced by numerical simulations of the complete spatiotemporal dynamics of the Josephson phase [57].

Note that these parametric phenomena can be used to create squeezed states of light [58]. As the Josephson coupling is sensitive to phase fluctuations, new experiments may become possible in which the fluctuations of the superconducting order parameter phase are controlled in the time domain, possibly stabilizing the superconducting state [2,3].

2.3. Josephson plasma solitons

Close to the JPR frequency, where the dielectric constant crosses zero, even small fields can drive the phase to very large amplitudes [29]. This was addressed experimentally in [30], using an intense narrowband THz source of a THz free electron laser with a central frequency ω_{FEL}, a bandwidth of $\Delta\omega_{\text{FEL}}/\omega_{\text{FEL}} \approx 1 - 2\%$, and continuously tunable in the vicinity of the JPR frequency $\omega_p \approx 2$ THz of the optimally doped $La_{1.84}Sr_{0.16}CuO_4$. Several phenomena were reported depending if the central frequency of the driving field is far above, close to, or slightly below the JPR, thereby establishing that the nonlinearities in the Josephson coupling get enhanced as ω_{FEL} is tuned into resonance with ω_p.

The most striking phenomenon corresponds to the case where the driving field is tuned slightly below the JPR. For a THz field strength corresponding to the linear excitation regime, the impinging electromagnetic wave is evanescent, penetrating within a length of the order of λ_c. Remarkably, above a certain threshold electric field, a solitonic propagating mode emerges (see Figure 15).

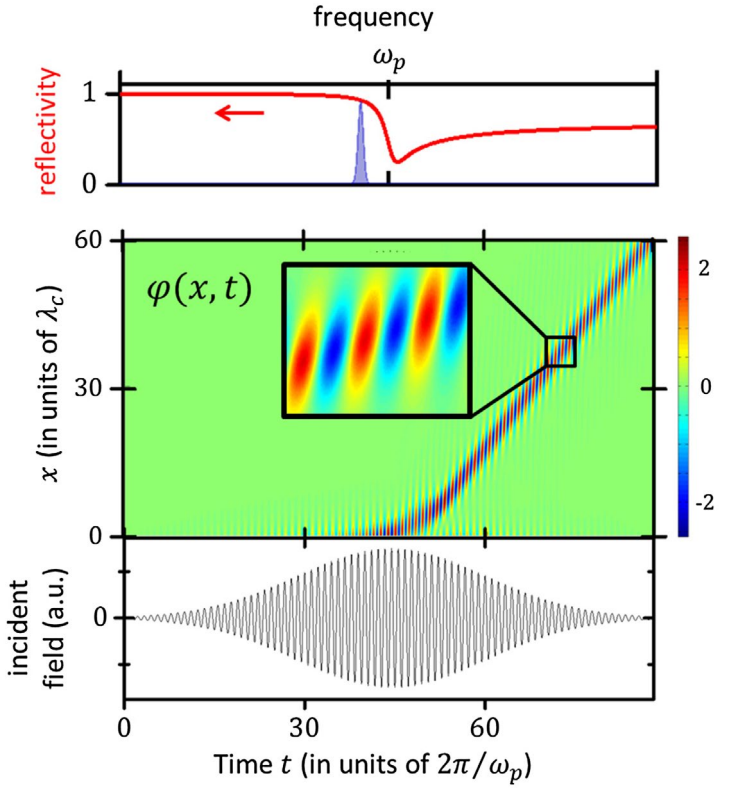

Figure 15. Simulations of the spatiotemporal dynamics of the Josephson phase $\varphi(x,t)$ after interaction with an intense narrowband THz pulse tuned slightly below the JPR. *Top panel*: Comparison between the Fourier spectrum of the THz pulse (purple area) and the JPR characterized by a plasma edge in the reflectivity (red curve). *Main panel*: two-dimensional color plot of the spatiotemporal evolution of $\varphi(x,t)$ showing the excitation of a Josephson plasma soliton. *Bottom panel*: incident electromagnetic field impinging on the surface of the superconductor.

This mode concentrates the electromagnetic energy in space and time without any noticeable distortion of its shape as it propagates. A more detailed visualization of its space–time evolution is presented in the inset of the main panel of Figure 15. This type of Josephson soliton corresponds to a vortex–anti-vortex pair that oscillates back and forth in time during its propagation, at a frequency $\sim \omega_p$, and is called a breather. The characteristics of the soliton, such as its precise shape, its speed, and its oscillation frequency, depend sensitively on the excitation conditions above threshold.

Experimentally, this type of solitonic excitation could be probed via the time- and frequency-dependent loss function $L(\omega,t)$. When the soliton forms and propagates within the superconductor, a strong change of the loss function is found, which is exponentially sensitive on field strength and wavelength and could only be reproduced qualitatively by numerical simulations. Figure 16 shows the experimental and simulated loss functions as a function of pump–probe delay, as well

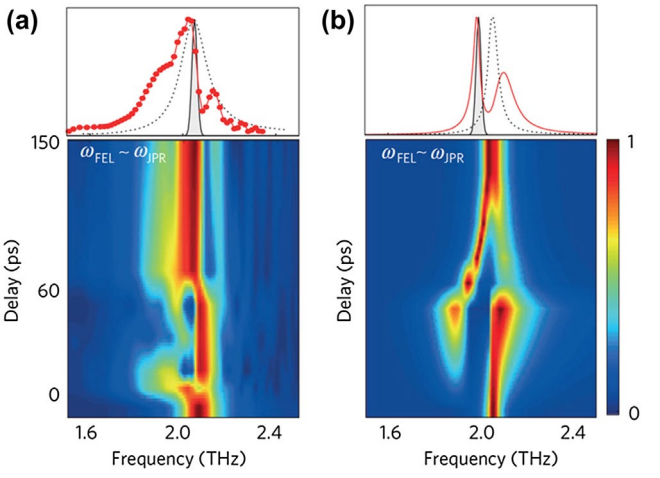

Figure 16. *Bottom panels*: Two-dimensional plots representing the time evolution of the frequency-resolved loss function as a function of pump–probe delay when a soliton is formed and propagates into the superconductor. Experimental (left) and simulated (right) loss functions are shown. *Top panels*: The figure shows the perturbed loss function for a line cut taken from the bottom panel at $t \sim 80$ ps (red curve), together with the equilibrium loss function (dotted black line) and with a Gaussian fit to the pump spectrum (gray, shaded). Reprinted from Dienst et al. [30].

as a line cut of the loss functions at $t = 80$ ps. The spectral reshaping, exhibiting a splitted lineshape and a dip, can be understood as a Fano-like lineshape [59–61], which results from the interaction between the soliton and the Josephson plasma waves that are employed to probe it.

3. Future directions: proposals for Josephson phase cooling

In the last part of this review, we discuss new strategies for the control of the Josephson plasma phenomena in cuprates. These works address the possibility to implement laser control schemes to manipulate the Josephson plasmons and to cool their fluctuations. The cooling schemes rely on energy transfer, mediated with light, between a low-frequency oscillator that is to be cooled (i.e. the Josephson oscillator here) and a high-frequency oscillator (Figure 17).

The high-frequency oscillator can either be an *internal* mode of the cuprate superconductor itself or an *external* one. We present both approaches in the following. In the first, the oscillator is *internal* and corresponds to the high-frequency intrabilayer Josephson plasma mode in bilayer cuprates such as YBCO. In the second, it is an *external* optical cavity that plays this role. The latter scheme is appropriate in cases where such an internal excitation doesn't exist, as in single layer cuprates such as $La_{2-x}Sr_xCuO_4$.

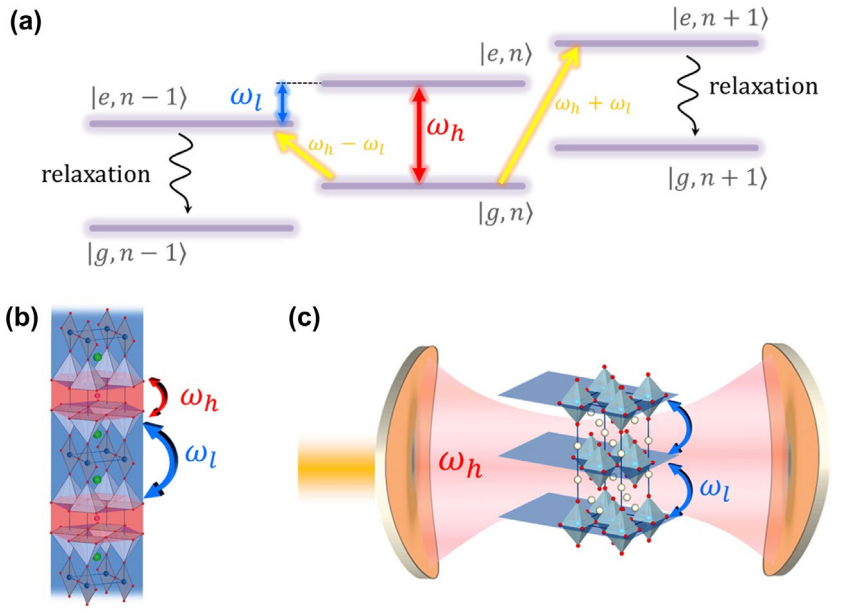

Figure 17. (a) Generic scheme for sideband cooling. $|g\rangle$ and $|e\rangle$ are the ground state and first excited state of the high-frequency oscillator, respectively (frequency ω_h), while $|n\rangle$ denotes the occupation number of the low-frequency oscillator (frequency ω_l). A laser (yellow arrows) tuned at $\omega_h - \omega_l$ (resp. $\omega_h + \omega_l$) provokes descending (resp. ascending) transitions, thereby decreasing (resp. increasing) the occupancy $|n\rangle$ of the low-frequency oscillator. (b) Crystal structure of the bilayer cuprate YBCO. Phase fluctuations can be transferred from the interbilayer (ω_l) to the intrabilayer (ω_h) Josephson junctions. (c) Sketch of a cavity cooling scheme. Josephson fluctuations of a single layer cuprate (ω_l) are transferred to the photonic mode of an optical cavity (ω_h).

3.1. *Parametric cooling of bilayer cuprates by THz excitation*

Bilayer cuprates have two superconducting layers per unit cell; hence, two types of Josephson junctions are connected in series: a thick and a thin one (see Figure 17(b)). These are characterized by their Josephson plasma frequencies ω_l (low frequency for the thick interbilayer junction) and ω_h (high frequency for the thin intrabilayer junction), with $\omega_l < \omega_h$. For a given temperature T such that $\hbar\omega_l < k_B T < \hbar\omega_h$, phase fluctuations in the interbilayer regions are more pronounced than in the intrabilayer ones. The model assumes that the dimensions of the superconductor in the *ab*-plane are much smaller than the magnetic penetration depth so that the dominant coupling mechanism between the junctions is capacitive and happens through a layer charging of the atomically thin superconducting electrodes. A parametric modulation of this coupling, which can be realized via a *c*-axis infrared lattice mode acting as a transducer, allows for the manipulation of the thermal populations of the junctions [62]. This happens when the modulation frequency ω_d matches the frequency of the two sidebands generated by the coupling between the interbilayer and the intrabilayer Josephson

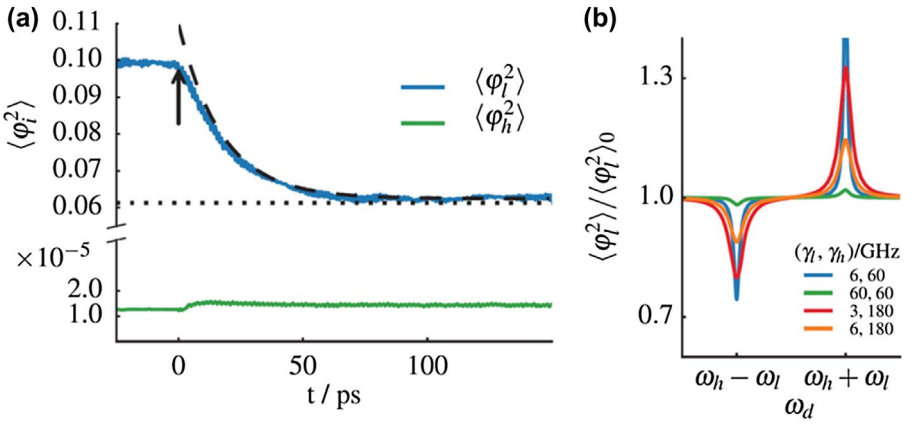

Figure 18. Parametric cooling in the two-junction case. The parameters taken for the simulation are: $\omega_l/2\pi = 1\text{THz}$ and $\omega_h/2\pi = 10\text{THz}$, $\gamma_l = 0.19\text{THz}$, $\gamma_h = 3.63\text{THz}$. (a) Time evolution of the Josephson phase fluctuations in the interbilayer and intrabilayer junctions ($\langle\varphi_l^2\rangle$ and $\langle\varphi_h^2\rangle$, respectively) after a resonant driving is turned on at $t = 0$ ps (the junctions are initially in thermal equilibrium). (b) Dependence of the cooling/heating effect as a function of the parametric modulation frequency ω_d for different sets of damping parameters. Reprinted with permission from Denny et al. [62]. Copyright 2015 by the American Physical Society.

junctions, which are given by $\omega_h - \omega_l = \omega_d$ and $\omega_h + \omega_l = \omega_d$ (see Figure 17(a)). Figure 18 shows the evolution of the thermal fluctuations of the phases (φ_l, φ_h) of two such coupled Josephson junctions, with dampings (γ_l, γ_h), in the parametrically driven regime for a representative set of parameters relevant for bilayer cuprates.

Suppression of the phase fluctuations $\langle\varphi_l^2\rangle$ of the low-frequency Josephson junction from their value at thermal equilibrium is observed once the driving at $\omega_d = \omega_h - \omega_l$ is switched on at $t = 0$ ps. Correspondingly, there is an increase in the phase fluctuations $\langle\varphi_h^2\rangle$ in the high-frequency Josephson junction. Because the quadratures $\langle\dot{\varphi}_l^2\rangle$ and $\langle\dot{\varphi}_h^2\rangle$ behave similarly as $\langle\varphi_l^2\rangle$ and $\langle\varphi_h^2\rangle$, respectively (not shown), this effect corresponds to a change in the effective temperatures of both junctions (as opposed to a squeezed thermal state which would reduce one quadrature at the expense of the other): in the present case, the final state corresponds to an interbilayer mode cooled to $T = 0.6T_{\text{inital}}$ while the intrabilayer mode is heated to $T = 1.2T_{\text{inital}}$, where T_{inital} is the bath temperature. Figure 18(b) shows the frequency dependence for different sets of dampings of the low- and high-frequency Josephson junctions. As expected from the previous discussion, the decrease (cooling) or increase (heating) in the phase fluctuations $\langle\varphi_l^2\rangle$ of the low-frequency Josephson junction happens only within a range where ω_d matches the frequency of the two sidebands.

Most importantly, the phenomenology exposed here remains valid when one considers a stack composed of several of these Josephson junctions connected in series and representative of a bulk bilayer superconductor [62]. Experimentally, the cooling phenomenon may be observed by measuring the switching current

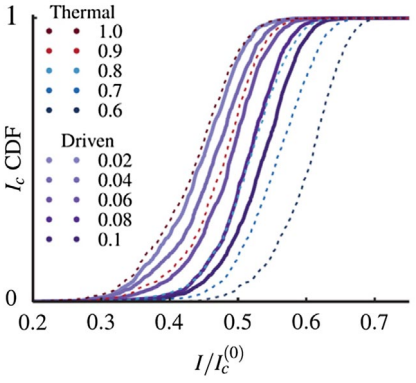

Figure 19. Cumulative distribution functions (CDF) of the switching current. The solid lines correspond to the driven states and the dotted lines correspond to thermal states. The reference thermal distribution at temperature T corresponds to the leftmost curve (brown dotted line). Thermal distributions at temperatures T' lower than T are shown ($T'/T = 0.6 \rightarrow 1.0$) as well as driven distributions with increasing driving strengths (0.02→0.1). Reprinted with permission from Denny et al. [62]. Copyright 2015 by the American Physical Society.

distribution of the stack. Figure 19 presents the cumulative distribution functions (CDF) of the switching current for a stack of 100 junctions for various thermal and driven states. The CDF associated with thermal distributions for different temperatures T' lower than a reference temperature T (T'/T from 0.6 to 1) shift toward higher switching currents with respect to the reference thermal distribution (the leftmost dotted line). Importantly, a similar trend is observed when the system is parametrically driven, starting from the equilibrium state at temperature T. Consequently, this points toward a remarkable similarity between the driven system and a thermal one of lower temperature.

3.2. Cavity Josephson plasmonics

Optical cavities have been used to 'dress' [63] and 'cool' [64,65] material excitations. To implement such an approach for manipulating Josephson plasmons in high-T_c cuprates, a design of THz cavities based on complex oxide heterostructuring [66,67] was proposed and is shown in Figure 20 [68].

The heterostructure involves a film of the single layer cuprate $La_{2-x}Sr_xCuO_4$, inserted between two insulating films of the parent compound La_2CuO_4, with a metallic oxide at the bottom (e.g. $SrRuO_3$) and metallic patches (e.g. gold) deposited on top of the structure. In this geometry, resonant THz modes are highly confined between the two metals, together with their electric field being polarized along the *c*-axis and propagation vector in the *ab*-plane [69]. Consequently, the THz photonic mode couples exclusively to the interlayer electrodynamic properties and to the JPR.

Without the high-T_c superconductor $La_{2-x}Sr_xCuO_4$ inside and for a given width w of the top metallic patches, the simulated reflectivity spectrum of the

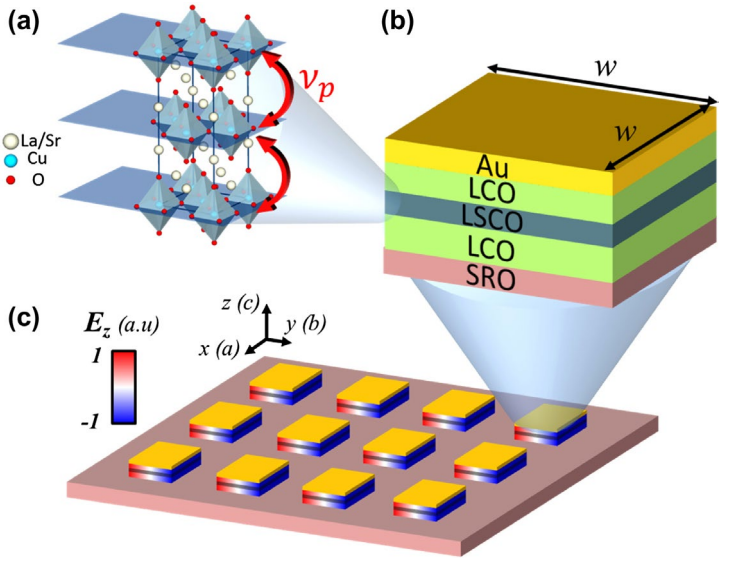

Figure 20. Proposed heterostructure for cavity Josephson plasmonics. (a) zoom on the high-T_c superconductor $La_{2-x}Sr_xCuO_4$. Red arrows indicate the Josephson plasma oscillations between the planes at the characteristic frequency ν_p. (b) zoom on a single THz cavity enclosing the high-T_c cuprate: Au/La_2CuO_4(LCO)/$La_{2-x}Sr_xCuO_4$(LSCO)/La_2CuO_4 (LCO)/$SrRuO_3$ (SRO). (c) the proposed heterostructure: an array of THz cavities grown from thin films and embedding an high-T_c cuprate. The electric field distribution of the fundamental mode of the 'bare' cavities (i.e. without the superconductor) is shown. Reprinted with permission from Laplace et al. [68]. Copyright 2016 by the American Physical Society.

heterostructure exhibits an absorption dip at a frequency $\nu_c(w)$, signaling the cavity resonance (see Figure 21(a), left panel). The spatial distribution of the electric field of the corresponding photonic mode is shown in Figure 20(c). As the cavity resonance depends on the inverse patch width, defined as $\nu(w) = c/(2\sqrt{\epsilon_\infty}w)$ ($\epsilon_\infty \approx 27$ being the dielectric constant of the insulating La_2CuO_4), precise tuning of the cavity can be achieved by varying the width of the top gold patches (Figure 21(a), right panel). When a superconducting film of the optimally doped $La_{2-x}Sr_xCuO_4$ with JPR frequency $\nu_p = 2.3$ THz is inserted inside the heterostructure, a qualitatively different behavior is observed. As the cavity resonance is swept through the JPR frequency, one observes a clear avoided crossing which indicates a strong coupling between the JPR and the THz photonic mode (Figure 21(b), right panel). At resonance ($\nu_c(w) = \nu_p$, Figure 21(b) left panel), the reflectivity signals the presence of two modes that are separated by a Rabi splitting 2Ω [70].This shows the possibility to dress the Josephson plasmons with the THz photonic mode of the cavity and to create hybridized Josephson plasmon–polariton excitations. Additionally, the energies of the two Josephson plasmon–polaritons can be tuned by varying the thickness of the superconducting film inside the structure [68].

When the THz cavities are tuned off resonantly with respect to the JPR, i.e. in a parametric regime, the Hamiltonian of the plasmon–cavity system writes [68]:

$$H = h\nu_c a^+ a + h\nu_p b^+ b + hg(b^+ + b)\, a^+ a$$

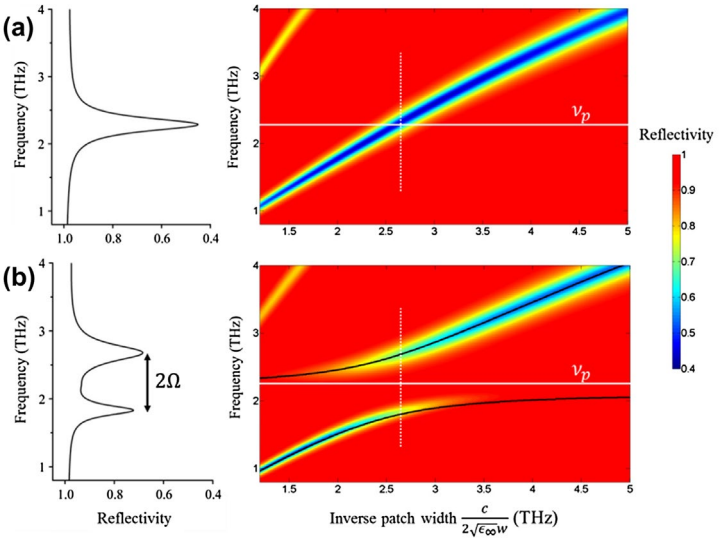

Figure 21. (a) *Right*: Reflectivity as a function of frequency and inverse patch width of the bare heterostructure. The white solid line shows the JPR frequency ν_p. *Left*: Reflectivity cut of the bare cavity tuned at ν_p (white dashed line on the right panel). (b) *Right*: Reflectivity as a function of frequency and inverse patch width for the cavity/high-T_c heterostructure. The white solid line shows the JPR frequency ν_p. *Left*: Reflectivity cut of the cavity/high-T_c heterostructure when the bare cavity is tuned at ν_p (white dashed line on the right panel). Reprinted with permission from Laplace et al. [68]. Copyright 2016 by the American Physical Society.

where a^+, a, b^+, and b are the creation and annihilation operators of the photon and Josephson plasmon fields, respectively, ν_c and ν_p are the cavity and JPR frequencies, and g is the coupling between the plasmons and the cavity mode. This Hamiltonian is the very same used in the context of cavity optomechanics to cool mechanical modes [65]; hence, it is proposed that these THz cavities can be used to control the dynamics of the Josephson plasmons and to cool their fluctuations. The cavity cooling scheme described here makes use of the nonlinearity of the Josephson effect, whereas the parametric cooling scheme of the previous section did not rely on it. Previously, the interbilayer and intrabilayer Josephson plasma modes formed a linearly coupled system and the up-conversion process was achieved by the modulation of the coupling between the two. Here, the light is inelastically scattered by the plasmons and the cavity resonance is used to select the anti-Stokes transition (i.e. to up-convert the photon energy), hence reducing the number of thermally excited plasmons. From the typical figures of merit determined for these cavities, it was estimated a threshold of the order of a few ten's of kV/cm for the incident THz field in order to observe cooling dynamics in this system [68]. This field strength is presently achievable with both table-top THz sources and Terahertz-free electron lasers.

4. Conclusion and outlook

As discussed in this review, Josephson plasma phenomena in high-T_c cuprates are associated with a wide range of scientific challenges, with fundamental and technological ramifications. We have drawn special attention to the possibility of controlling the Josephson plasma modes in a coherent and non-dissipative fashion, enabled by the recent development of intense THz light pulses, both table-top and at free-electron lasers. Based on the diversity of the plasma modes arising from the Josephson coupling which have not been addressed experimentally yet (e.g. surface Josephson plasma modes, plasma modes in restricted geometries, and Josephson plasma modes engineered with cavities), many new possibilities remain unexplored. Finally, we pointed out that advanced schemes can be envisaged in which these collective modes are manipulated, including schemes in which their fluctuations are cooled with light.

Disclosure statement

No potential conflict of interest was reported by the authors.

Funding

This work was supported by the European Research Council under the European Union's Seventh Framework Programme (FP7/2007-2013)/ERC Grant Agreement number 319286 (Q-MAC).

References

[1] J.G. Bednorz and K.A. Müller, Z. Phys. B. 64 (1986) p.189.
[2] V. Emery and S. Kivelson, Nature 374 (1995) p.434.
[3] Z.A. Xu, N.P. Ong, Y. Wang, T. Kakeshita and S. Uchida, Nature 406 (2000) p.486.
[4] K. Tamasaku, Y. Nakamura and S. Uchida, Phys. Rev. Lett. 69 (1992) p.1455.
[5] R. Kleiner, F. Steinmeyer, G. Kunkel and P. Müller, Phys. Rev. Lett. 68 (1992) p.2394.
[6] R. Kleiner and P. Müller, Phys. Rev. B 49 (1994) p.1327.
[7] K. Inomata, S. Sato, K. Nakajima, A. Tanaka, Y. Takano, H.B. Wang, M. Nagao, H. Hatano and S. Kawabata, Phys. Rev. Lett. 95 (2005) p.107005.
[8] X.Y. Jin, J. Lisenfeld, Y. Koval, A. Lukashenko, A.V. Ustinov and P. Müller, Phys. Rev. Lett. 96 (2006) p.177003.
[9] W.E. Lawrence and S. Doniach, in *Proceedings 12th International Conference of Low Temperature Physics*, E. Kanda ed., Keigaku Publishing, Tokyo, 1971, p.361.
[10] A. Barone and G. Paternò, *Physics and Applications of the Josephson Effect*, John Wiley & Sons Inc., 1982.
[11] R. Kleiner, P. Müller, H. Kohlstedt, N.F. Pedersen and S. Sakai, Phys. Rev. B 50 (1994) p.3942.
[12] L.N. Bulaevskii, M. Zamora, D. Baeriswyl, H. Beck and J.R. Clem, Phys. Rev. B 50 (1994) p.12831.
[13] Hu Xiao and Shi-Zeng Lin, Supercond. Sci. Tech. 23 (2010) p.053001.

[14] S.E. Savel'ev, V.A. Yampol'skii, A.L. Rakhmanov, F. Nori. Rep. Prog. in Phys. 73 (2010) p.026501.
[15] J.M. Rowell, Phys. Rev. Lett. 11 (1963) p.200.
[16] G. Blatter, M.V. Feigel'man, V.B. Geshkenbein, A.I. Larkin and V.M. Vinokur, Rev. Mod. Phys. 66 (1994 – Published 1 October) p.1125.
[17] A.E. Koshelev and M.J.W. Dodgson, Zh. Eksp. Teor. Fiz. 144(9) (2013) p.519 [JETP 117, 450 (2013)].
[18] T. Kashiwagi, M. Tsujimoto, T. Yamamoto, H. Minami, K. Yamaki, K. Delfanazari, K. Deguchi, N. Orita, T. Koike, R. Nakayama, T. Kitamura, M. Sawamura, S. Hagino, K. Ishida, K. Ivanovic, H. Asai, M. Tachiki, R.A. Klemm, and K. Kadowaki, Jpn. J. Appl. Phys. 51 (2012) p.010113.
[19] K. Kadowaki and R. Kleiner, Nat. Photonics 7 (2013) p.702.
[20] L.N. Bulaevskii and A.E. Koshelev, Phys. Rev. Lett. 99 (2007) p.057002.
[21] L.N. Bulaevskii, A.E. Koshelev and M. Tachiki, Phys. Rev. B 78 (2008) p.224519.
[22] A.E. Koshelev and L.N. Bulaevskii, Phys. Rev. B 77 (2008) p.014530.
[23] S. Lin and X. Hu, Phys. Rev. Lett. 100 (2008) p.247006.
[24] A.E. Koshelev, Phys. Rev. B 78 (2008) p.174509.
[25] Hu Xiao and Shizeng Lin, Phys. Rev. B. 80 (2009) p.064516.
[26] R.A. Klemm and K. Kadowaki, J. Phys.: Condens. Matter. 22 (2010) p.375701.
[27] S.-Z. Lin and X. Hu, Phys. Rev. B 82 (2010) p.020504(R).
[28] L. Ozyuzer, A.E. Koshelev, C. Kurter, N. Gopalsami, Q. Li, M. Tachiki, K. Kadowaki, T. Yamamoto, H. Minami, H. Yamaguchi, T. Tachiki, K.E. Gray, W.-K. Kwok and U. Welp, Science 318 (2007) p.1291.
[29] S. Savel'ev, A.L. Rakhmanov, V.A. Yampol'skii and F. Nori. Nat. Phys. 2 (2006) p.521.
[30] A. Dienst, E. Casandruc, D. Fausti, L. Zhang, M. Eckstein, M. Hoffmann, V. Khanna, N. Dean, M. Gensch, S. Winnerl, W. Seidel, S. Pyon, T. Takayama, H. Takagi and A. Cavalleri, Nat. Mater. 12 (2013) p.535.
[31] V.K. Thorsmølle, R.D. Averitt, M.P. Maley, L.N. Bulaevskii, C. Helm and A.J. Taylor, Opt. Lett. 26 (2001) p.1292.
[32] S.V. Dordevic, S. Komiya, Y. Ando and D.N. Basov, Phys. Rev. Lett. 91 (2003) p.167401.
[33] D. van der Marel and A.A. Tsvetkov, Czech. J. Phys. 46 (1996) p.3165.
[34] D. van der Marel and A.A. Tsvetkov, Phys. Rev. B 64 (2001– Published 22 June) p.024530.
[35] H. Shibata and T. Yamada, Phys. Rev. Lett. 81 (1998 – Published 19 October) p.3519.
[36] D. Munzar and M. Cardona, Phys. Rev. Lett. 90 (2003– Published 18 February) p.077001.
[37] Y. Hirata, K.M. Kojima, M. Ishikado, S. Uchida, A. Iyo and H. Eisakiand S. Tajima, Phys. Rev. B 85 (2012– Published 2 February) p.054501.
[38] A. Dubroka, M. Rössle, K.W. Kim, V.K. Malik, D. Munzar, D.N. Basov, A.A. Schafgans, S.J. Moon, C.T. Lin, D. Haug, V. Hinkov, B. Keimer, Th Wolf, J.G. Storey, J.L. Tallon and C. Bernhard, Phys. Rev. Lett. 106 (2011 – Published 27 January) p.047006.
[39] W. Hu, S. Kaiser, D. Nicoletti, C.R. Hunt, I. Gierz, M.C. Hoffmann, M. Le Tacon, T. Loew, B. Keimer and A. Cavalleri, Nat. Mater. 13 (2014) p.705–711.
[40] S. Kaiser, C.R. Hunt, D. Nicoletti, W. Hu, I. Gierz, H.Y. Liu, M. Le Tacon, T. Loew, D. Haug, B. Keimer and A. Cavalleri, Phys. Rev. B 89 (2014 – Published 30 May) p.184516.
[41] R. Mankowsky, A. Subedi, M. Först, S.O. Mariager, M. Chollet, H. Lemke, J. Robinson, J. Glownia, M. Minitti, A. Frano, M. Fechner, N.A. Spaldin, T. Loew, B. Keimer, A. Georges and A. Cavalleri, Nature 516 (2014) p.71.
[42] T.M. Slipchenko, D.V. Kadygrob D. Bogdanis, V.A. Yampol'skii and A.A. Krokhin, Phys. Rev. B 84 (2011) p.224512.
[43] V.A. Yampol'skii, A.V. Kats, M.L. Nesterov, A.Y. Nikitin, T.M. Slipchenko, S. Savel'ev and F. Nori. Phys. Rev. B. 76 (2007) p.224504.

[44] V.A. Yampol'skii, A.V. Kats, M.L. Nesterov, A.Y. Nikitin, T.M. Slipchenko, S. Savel'ev and F. Nori. Phys. Rev. B. 79 (2009) p.214501.
[45] H.T. Stinson, J.S. Wu, B.Y. Jiang, Z. Fei, A.S. Rodin, B.C. Chapler, A.S. McLeod, A. Castro Neto, Y.S. Lee, M.M. Fogler and D.N. Basov, Phys. Rev. B 90 (2014) p.014502.
[46] F. Alpeggiani and L.C. Andreani, Phys. Rev. B 88 (2013) p.174513.
[47] S. Savel'ev, A.L. Rakhmanov and F. Nori. Phys. Rev. Lett. 94 (2005) p.157004.
[48] A. Wall-Clarke and S. Savel'ev. Phys. Rev. B. 85 (2012) p.214521.
[49] A.L. Rakhmanov, V.A. Yampol'skii, J.A. Fan, F. Capasso and F. Nori, Phys. Rev. B 81 (2010) p.075101.
[50] V.A. Yampol'skii, S. Savel'ev, A.L. Rakhmanov, and F. Nori. Phys. Rev. B. 78 (2008) p.024511.
[51] S.S. Apostolov, Z.A. Maizelis and M.A. Sorokina, V.A. Yampol'skii and F. Nori, Phys. Rev. B 82 (2010) p.144521.
[52] F. Alpeggiani, Opt. Lett. 40 (2015) p.867.
[53] A.A. Schafgans, A.D. LaForge, S.V. Dordevic, M.M. Qazilbash, W.J. Padilla, K.S. Burch and Z.Q. Li, S. Komiya, Y. Ando and D.N. Basov, Phys. Rev. Lett. 104 (2010) p.157002.
[54] S.V. Dordevic, S. Komiya, Y. Ando, Y.J. Wang and D.N. Basov, Phys. Rev. B 71 (2005) p.054503.
[55] J. Hebling, K.-L. Yeh, M.C. Hoffmann, B. Bartal and K.A. Nelson, J. Opt. Soc. of Amer. B 25 (2008) p.B6.
[56] A.Dienst, M.C. Hoffmann, D. Fausti, J.C. Petersen, S. Pyon, T. Takayama, H. Takagi and A. Cavalleri, Nat. Photonics 5 (2011) p.485.
[57] S. Rajasekaran, E. Casandruc, Y. Laplace, D. Nicoletti, G.D. Gu, S.R. Clark, D. Jaksch and A. Cavalleri, Nat. Phys. (2016). doi:http://dx.doi.org/10.1038/nphys3819. Advance online publication.
[58] L.-A. Wu, M. Xiao and H.J. Kimble, J. Opt. Soc. Amer. B 4 (1987) p.1465.
[59] U. Fano, Phys. Rev. 124 (1961) p.1866.
[60] K.-J. Boller, A. Imamoğlu and S.E. Harris, Phys. Rev. Lett. 66 (1991) p.2593.
[61] A.A. Abdumalikov Jr., O. Astafiev, A.M. Zagoskin, Y.A. Pashkin and Y. Nakamura and J.S. Tsai, Phys. Rev. Lett. 104 (2010) p.193601.
[62] S.J. Denny, S.R. Clark, Y. Laplace, A. Cavalleri and D. Jaksch, Phys. Rev. Lett. 114 (2015) p.137001.
[63] J. Kasprzak, M. Richard, S. Kundermann, A. Baas, P. Jeambrun, J.M.J. Keeling, F.M. Marchetti, M.H. Szymańska, R. André, J.L. Staehli, V. Savona, P.B. Littlewood, B. Deveaud and L.S. Dang, Nature 443 (2006) p.409.
[64] J. Hammer, M. Aprili and I. Petković, Phys. Rev. Lett. 107 (2011) p.017001.
[65] Markus Aspelmeyer, T.J. Kippenberg and F. Marquardt, Rev. Mod. Phys. 86 (2014) p.1391.
[66] J. Mannhart and D.G. Schlom, Science 327 (2010) p.1607.
[67] P. Zubko, S. Gariglio, M. Gabay, P. Ghosez and Jean-Marc Triscone, Ann. Rev. Condens. Matter Phys. 2 (2011) p.141.
[68] Y. Laplace, S. Fernandez-Pena, S. Gariglio, J.M. Triscone and A. Cavalleri, Phys. Rev. B 93 (2016) p.075152.
[69] Y. Todorov, L. Tosetto, J. Teissier, A.M. Andrews, P. Klang, R. Colombelli, I. Sagnes, G. Strasser and C. Sirtori, Opt. Express 18 (2010) p.13886.
[70] G. Khitrova, H.M. Gibbs, F. Jahnke, M. Kira and S.W. Koch Rev. Mod. Phys. 71 (1999) p.1591.